Membrane Fluidity and Lipid Order in Ternary Giant Unilamellar Vesicles Using a New Bodipy-Cholesterol Derivative

Florly S. Ariola,[†] Zaiguo Li,[‡] Christine Cornejo,[†] Robert Bittman,[‡] and Ahmed A. Heikal[†§*]

[†]Department of Bioengineering, The Pennsylvania State University, University Park, Pennsylvania; [‡]Department of Chemistry and Biochemistry, Queens College of the City University of New York, Flushing, New York; and [§]The Huck Institutes of the Life Sciences, The Pennsylvania State University, University Park, Pennsylvania

ABSTRACT Cholesterol-rich, liquid-ordered (L_o) domains are believed to be biologically relevant, and yet detailed knowledge about them, especially in live cells under physiological conditions, is elusive. Although these domains have been observed in model membranes, understanding cholesterol-lipid interactions at the molecular level, under controlled lipid mixing, remains a challenge. Further, although there are a number of fluorescent lipid analogs that partition into liquid-disordered (L_d) domains, the number of such analogs with a high affinity for biologically relevant L_o domains is limited. Here, we use a new Bodipy-labeled cholesterol (Bdp-Chol) derivative to investigate membrane fluidity, lipid order, and partitioning in various lipid phases in giant unilamellar vesicles (GUVs) as a model system. GUVs were prepared from mixtures of various molar fractions of dioleoylphosphatidylcholine, cholesterol, and egg sphingomyelin. The L_d phase domains were also labeled with 1,1′-didodecyl-3,3,3′,3′-tetramethylindocarbocyanine (DiI-C_{12}) for comparison. Two-photon fluorescence lifetime and anisotropy imaging of Bdp-Chol are sensitive to lipid phase domains in GUVs. The fluorescence lifetime of Bdp-Chol in liquid-disordered, single-phase GUVs is 5.50 $\pm$ 0.08 ns, compared with 4.1 $\pm$ 0.4 ns in the presence of DiI-C_{12}. The observed reduction of fluorescence lifetime is attributed to Förster resonance energy transfer between Bdp-Chol (a donor) and DiI-C_{12} (an acceptor) with an estimated efficiency of 0.25 and donor-acceptor distance of 2.6 $\pm$ 0.2 nm. These results also indicate preferential partitioning ($K_p = 1.88$) of Bdp-Chol into the L_o phase. One-photon, time-resolved fluorescence anisotropy of Bdp-Chol decays as a triexponential in the lipid bilayer with an average rotational diffusion coefficient, lipid order parameter, and membrane fluidity that are sensitive to phase domains. The translational diffusion coefficient of Bdp-Chol, as measured using fluorescence correlation spectroscopy, is (7.4 $\pm$ 0.3) $\times$ 10^{-8} cm^2/s and (5.0 $\pm$ 0.2) $\times$ 10^{-8} cm^2/s in the L_d and L_o phases, respectively. Experimental translational/rotational diffusion coefficient ratios are compared with theoretical predictions using the hydrodynamic model (Saffman-Delbrück). The results suggest that Bdp-Chol is likely to form a complex with other lipid molecules during its macroscopic diffusion in GUV lipid bilayers at room temperature. Our integrated, multiscale results demonstrate the potential of this cholesterol analog for studying lipid-lipid interactions, lipid order, and membrane fluidity of biologically relevant L_o domains.

INTRODUCTION

Giant unilamellar vesicles (GUVs) serve as cell-size model systems for studying many aspects of biological membranes under controlled changes of thermodynamic parameters. Lipid domains, most notably the liquid-ordered (L_o) domain, have been widely studied in model membranes because of their potential role in various cellular mechanisms including signal transduction, cellular transport, and membrane fusion (1–3). Based on the thermodynamics of lipid mixing, the ability to predict the formation of specific lipid domains is of particular interest (4). Fluorescence microscopy and spectroscopy have been used to understand lipid-lipid, lipid-protein, and/or lipid-marker interactions in these microdomains (5–10). However, the use of lipid analogs for membrane studies is limited by their ability to partition into specific (mostly liquid-disordered (L_d)) domains because of their chemical structures (3,11). Developing new fluorescent lipid analogs for biologically relevant L_o domains (also known as ''lipid rafts'') remains a challenge, as is evident from the limited number of choices currently available. Related fluorescence-atomic force microscopy studies have shown that the attachment of a bulky chromophore, such as 1,6-diphenylhexatriene or Bodipy, to saturated acyl chains results in a decreased affinity for more ordered domains (11). Additionally, one of the outstanding questions in membrane studies is whether cholesterol diffuses freely in a lipid bilayer or as a complex (even transiently) with other lipid molecules (4,12,13). Verifying the sensitivity of such cholesterol-lipid cluster formations to lipid phase/type also remains a challenge.

Recently, Bittman and co-workers (14) synthesized a cholesterol-Bodipy (Bdp-Chol) derivative (Fig. 1 *A*) and demonstrated that it partitions into the L_o phase of bilayers. By comparison, 7-nitrobenz-2-oxa-1,3-diazole and dansyl derivatives in model membranes favor the L_d phase because of the chemical nature of the chromophore link to cholesterol, the fluorophore size, and/or the chromophore polarity. In contrast, Bdp-Chol more closely mimics cholesterol due to the apolar nature of the fluorophore (15) and the absence of polar atoms in the aliphatic side chain that links the Bodipy moiety to cholesterol (11). In addition, Bodipy exhibits desirable photophysical properties, such as a high extinction coefficient (~90,000 M^{-1} cm^{-1}), fluorescence quantum yield

Submitted April 12, 2008, and accepted for publication December 17, 2008.

*Correspondence: aah12@psu.edu

Editor: Joshua Zimmerberg.

0006-3495/09/04/2696/13 $2.00

doi: 10.1016/j.bpj.2008.12.3922

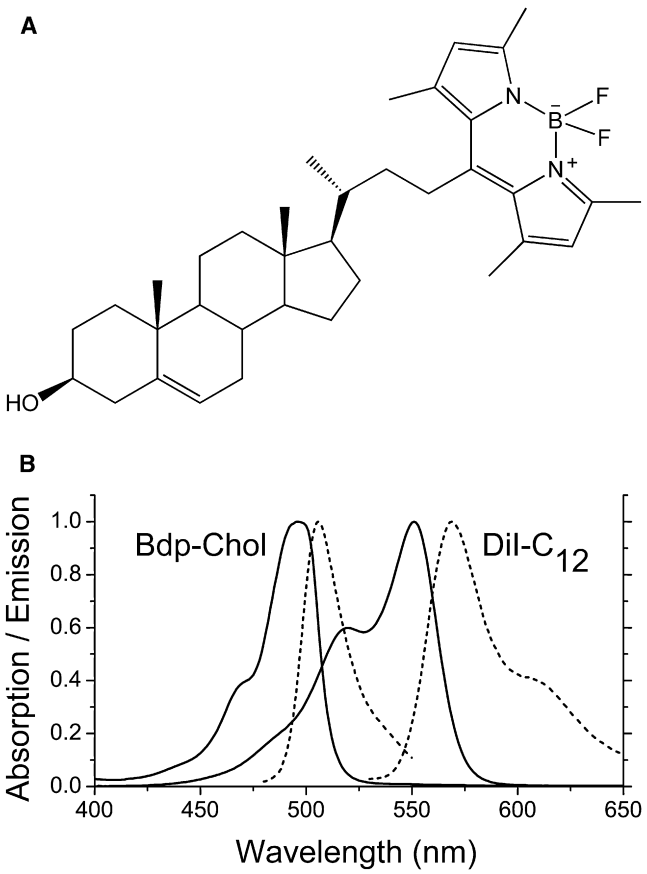

FIGURE 1 Chemical structure of Bdp-Chol and steady-state spectroscopy of lipid analogs used in these studies. (*A*) The chemical structure of Bdp-Chol. (*B*) The normalized absorption (*solid line*) and emission (*dotted line*) spectra of Bdp-Chol and DiI-C_{12} (DMSO) indicate their potential as a donor-acceptor FRET pair in lipid bilayers.

(~0.8), and photostability, with an electronic transition dipole that is polarized along its long axis (15,16).

In this contribution, we explore Bdp-Chol fluorescence dynamics and interactions with lipid bilayers in ternary-phase GUVs as a model system. We use fluorescence lifetime and anisotropy measurements of Bdp-Chol to probe the lipid order and membrane fluidity in different domains with high spatial and temporal resolution. We quantified the partitioning of Bdp-Chol in ternary mixtures of dioleoylphosphatidylcholine (DOPC)/egg sphingomyelin (SM)/cholesterol using the Förster resonance energy transfer (FRET) method. Our results show that Bdp-Chol preferentially partitions into both the L_o and L_d phase domains as compared with the gel phase (L_β). We also used time-resolved fluorescence anisotropy and fluorescence correlation spectroscopy (FCS) to assess whether Bdp-Chol diffuses freely in the lipid bilayer or forms complexes with other lipid molecules during translational diffusion (17). The fluorescence and partitioning properties of Bdp-Chol can be exploited in membrane domain studies below the diffraction limit.

MATERIALS AND METHODS

Materials

DOPC, cholesterol, and egg SM were purchased from Avanti Polar Lipids (Alabaster, AL). All lipid solutions were stored at −20°C as a 10 mg/mL stock solution in spectroscopic-grade chloroform (EMD Chemicals, Gibbstown, NJ). Bdp-Chol (Fig. 1 *A*), synthesized as described by Li et al. (14), absorbs ~ 496 nm, with maximum emission at 506 nm in dimethyl sulfoxide (DMSO) (Fig. 1 *B*). As a label for the L_d phase domain, 1,1′-didodecyl-3,3,3′,3′-tetramethylindocarbocyanine perchlorate (DiI-C_{12}) was purchased from Invitrogen (Carlsbad, CA). The absorption and emission bands of DiI-C_{12} (in DMSO) are centered at 551 nm and 659 nm, respectively (Fig. 1 *B*). Fluorophores were stored at −20°C as a 1 mg/mL stock solution in spectroscopic-grade methanol (Burdick & Jackson, Muskegon, MI). For quenching experiments, trypan blue was used as purchased from ATCC (Manassas, VA). Rhodamine green (RhG; Invitrogen), with a diffusion coefficient $D_T \sim 2.8 \times 10^{-6}$ cm^2/s, was used to calibrate our FCS system (18).

Preparation of GUVs

GUVs were prepared by electroformation, as previously described (5). Briefly, various lipid compositions (Table 1) were used for lipid mixing to generate and manipulate lipid phase domains. Lipids were dissolved in a 9:1 mixture of chloroform/methanol (v/v). Lipid solutions were deposited on electrodes and dried under vacuum. The lipid film on the electrodes was rehydrated in a cell containing a 50-mM sucrose solution heated to 55°C. The electroformation cell was then connected to a function generator and placed in a 55°C oven for the duration of the electroformation process. The resulting GUVs were then prepared on sealed slides, where the vesicles were used for the reported measurements (at room temperature, 22°C) within one day of formation. For quenching experiments, two slides were prepared from the same GUV sample with (0.0075% w/v) and without trypan blue before confocal imaging of Bdp-Chol under the same conditions.

Microscopy and ultrafast spectroscopy

The experimental set-up used for fluorescence lifetime and anisotropy measurements has been described previously in detail (5,6,18). The laser scanning confocal microscope (Olympus, Melville, NY) consists of an inverted microscope (IX81), a scanning unit (FV300), and a 1.2 NA, 60× water-immersion objective. The confocal system was modified to accommodate two-photon (2P) fluorescence lifetime imaging (FLIM) and polarization imaging of Bdp-Chol using 960-nm femtosecond laser pulses, which are

TABLE 1 Molar fractions of lipid mixing (DOPC/sphingomyelin/cholesterol) used for GUVs

Lipid composition	DOPC (mol %)	Sphingomyelin (mol %)	Cholesterol (mol %)	Lipid analog	Lipid phase
A	100	—	—	Bdp-Chol	L_d
B	50	50	—	Bdp-Chol, DiI-C_{12}	L_d–L_β†
C	—	100	—	Bdp-Chol	L_β
D	70	10	20	Bdp-Chol	L_o
E	25	55	20	Bdp-Chol, DiI-C_{12}*	L_o–L_d
F	25	50	25	Bdp-Chol, DiI-C_{12}	L_o–L_d
G	25	40	35	Bdp-Chol, DiI-C_{12}	L_o–L_d

GUVs were prepared according to the phase diagram shown in Fig. 2.
*With DiI-C_{12} present in the L_d phase, the fluorescence excitation and detection conditions were optimized for Bdp-Chol.
†L_d and L_β phase coexistence.

generated by a titanium-sapphire laser system (Mira 900-F, Coherent, Santa Clara, CA). The second harmonic (480 nm) was used for complementary one-photon (1P) excitation experiments at a reduced repetition rate (4.2 MHz, Mira 9200, Coherent). The epifluorescence signal was directed toward two microchannel plate photomultiplier tubes (R3809U, Hamamatsu, Hamamatsu City, Japan) through two Glan-Thompson polarizers using a 50/50 beam splitter. A histogram of fluorescence photon arrival times (i.e., a fluorescence decay) was recorded using an SPC 830 module (Becker and Hickl, Berlin, Germany) (19).

For confocal images, a 488-nm fiber-coupled CW laser was used to excite Bdp-Chol, with its emission collected via a 525 ± 15-nm bandpass (BP) filter. DiI-C_{12} was excited with a 543-nm laser and its emission was collected with a 605/70 BP filter. A 525 ± 25-nm bandpass emission filter was used for single-point, 1P fluorescence lifetime and anisotropy measurements of Bdp-Chol. For 2P fluorescence imaging of Bdp-Chol, an additional 690-nm short-pass filter was also used (along with a 525/50 BP filter) to further suppress any infrared laser scattering.

Data analysis

Based on the chromophore structure and the surrounding lipid phase, the magic-angle fluorescence intensity decay ($I_{54.7}$) of a chromophore is generally described (5,6,18,20) as

$$I_{54.7}(x,y,t) = \sum_{i=1}^{2} \alpha_i(x,y)\exp[-t/\tau_i(x,y)]. \quad (1)$$

The time constants (τ_i) and amplitudes (α_i) were used to calculate the average fluorescence lifetime, $\bar{\tau}_{fl} = \sum_{i=1}^{2} \alpha_i\tau_i / \sum \alpha_i$. We used two operational modes of time-correlated single-photon counting (TCSPC): one with 2P laser scanning (i.e., 2P FLIM) and another where the 1P excitation laser was strategically focused (in an area of ~0.7 μm^2) on a selected lipid domain. In 2P FLIM, 256 × 256 pixels were used with 64 time bins/pixel (at 259 ps/bin). Complementary single-point measurements provided higher temporal resolution (1024 time bins at 24.4 ps/bin). A nonlinear least-square fitting routine (SPCImage, Becker & Hickl) was used to analyze fluorescence decays, deconvoluted with the system response function (full width at half-maximum ~50 ps). The residual and reduced χ^2 values (1.0–1.3) were used to assess the goodness of the fit.

The fluorescence anisotropy $r(x, y, t)$ of Bdp-Chol, at a given pixel (x,y) in a vesicle, was calculated using simultaneously measured parallel ($I_{\parallel}(x, y, t)$) and perpendicular ($I_{\perp}(x, y, t)$) fluorescence polarization images such that (5,6,18)

$$r(x,y,t) = \frac{[I_{//}(x,y,t) - G \times I_{\perp}(x,y,t)]}{[I_{//}(x,y,t) + 2G \times I_{\perp}(x,y,t)]} = \sum_{i=1}^{3} \beta_i(x,y)\exp[-t/\varphi_i(x,y)], \quad (2)$$

where the sum of preexponential factors (β_i) equals the initial anisotropy (r_0), which is sensitive to depolarization due to rotational diffusion and ultrafast energy transfer (20). The G-factor accounts for the biased detection efficiency due to polarization and is estimated ($G \sim 0.61$) using the tail-matching approach (20) on fluorescein ($\tau_{fl} = 3.9$ ns, $\varphi = 130$ ps, $r_0 = 0.33$). The initial anisotropy depends on the orientation angle (δ) between the absorbing and emitting dipoles (20,21) such that the maximum theoretical value of r_0 is 0.40 (for 1P) and 0.57 (for 2P) (20). Careful analysis of scattered light, G-factor, and optical depolarization due to the high NA objective (22,23) are critical for meaningful steady-state anisotropy images. According to the Stokes-Einstein model, the rotational time (φ) and diffusion coefficient (D_R) of a spherical fluorophore depend on its hydrodynamic volume (V) and surrounding viscosity (η) such that $D_R = 1/6\,\varphi = k_BT/6\,\eta V$ (20). The anisotropy decays were analyzed using OriginPro 7 (Origin Lab, Northampton, MA) and the fit goodness was judged by both the residual (not shown) and χ^2 (≤ 0.001).

FRET between two fluorophores can provide insights into donor and acceptor partitioning in lipid domains of a bilayer. In time-resolved FRET, the energy transfer efficiency ($E = 1 - \tau_{da}/\tau_d$) can also be calculated using the measured fluorescence lifetime for the donor with (τ_{da}) and without (τ_d) the presence of an acceptor (20). In membranes with translational phase separation, the fluorescence decay of the donor, in the presence of an acceptor, is given by (24)

$$I_{da}(t) = A_1\exp(-t/\tau_1)\exp\left(-c_1t^{1/3}\right) + A_2\exp(-t/\tau_2)\exp\left(-c_2t^{1/3}\right), \quad (3)$$

where τ_i is the donor excited-state lifetime in the ith lipid phase ($i = 1$ and 2 for the L_o and L_d phases, respectively), and c_1 is proportional to the surface density of acceptor molecules. The preexponential factors, A_i, are proportional to the number of donor molecules in the ith phase. The partition coefficient of a probe between lipid phases 1 and 2 is given by (24)

$$K_p = \frac{P_2/X_2}{P_1/X_1}, \quad (4)$$

where P_i is the probe mole fraction in the ith lipid phase and X_i is the corresponding mole fraction of the lipid phase. Using time-domain FRET, the partition coefficients of donor (K_p^d) and acceptor (K_p^a) probes can be calculated as (24)

$$K_p^d = \frac{A_2/X_2}{A_1/X_1} \quad (5)$$

$$K_p^a = \frac{c_2 \times a_2}{c_1 \times a_1}, \quad (6)$$

where a_i is the area/lipid molecule in the ith phase. The area/lipid molecule used in these calculations is taken from published molecular dynamics simulation studies (24–26). Here, we treat phase 1 as the L_o phase and phase 2 as the L_d phase.

Fluorescence correlation spectroscopy

The FCS setup has been described in detail elsewhere (18). FCS enables us to extend our observation time (10^{-6}–10 s) for translational diffusion studies using fluorescence fluctuations of single molecules (10^{-11}–10^{-9} M) as they diffuse throughout an open observation volume (27). Briefly, the sample is excited using high-repetition rate laser pulses (480 nm, 76 MHz) and the epifluorescence is isolated from the excitation light using a dichroic mirror (690 nm long-pass) plus a filter (525/50 bandpass) for Bdp-Chol emission. The fluorescence fluctuation signal from an open observation volume (~10^{-15} L) is then focused on an optical fiber (50 μm in diameter), which acts as a confocal pinhole before detection by an avalanche photodiode (APD, SPCM CD-2969, Perkin-Elmer, Fremont, CA). The signals are then autocorrelated using an external multiple-τ-digital correlator (ALV/6010-160, Langen/Hessen, Germany). The system is routinely calibrated using a photostable fluorophore, RhG, with a known translational diffusion coefficient ($D_T \sim 2.8 \times 10^{-6}$ cm^2/s) (27–29).

The autocorrelation function, $G(\tau)$, of fluorescence fluctuation, $\delta F(t)$, is defined as (27,28,30) $G_D(\tau) = [\delta F(t) \times \delta F(t+\tau)] / \langle F(t)\rangle^2$, where $F(t)$ is the fluorescence intensity at time t. The autocorrelation of fluorescence fluctuations of a single species diffusing in three dimensions (3D) is given by (27,28,30)

$$G_D(\tau) = N^{-1}(1 + \tau/\tau_D)^{-1}\left(1 + \tau/\omega_0^2\tau_D\right)^{-0.5}. \quad (7)$$

The corresponding autocorrelation function for a diffusing fluorophore in a lipid bilayer (i.e., in 2D) is given by (31,32)

$$G_D(\tau) = N^{-1}(1 + \tau/\tau_D)^{-1}, \quad (8)$$

where N is the average number of molecules diffusing in an open 3D Gaussian observation volume with an axial/translational dimension ratio $\omega_0 = z / \omega_{xy}$. The diffusion time ($\tau_D$), which is the average residence time of a diffusing molecule through an observation volume, is used to calculate the translational diffusion coefficient (D_T) where $\tau_D = \omega_{xy}^2/4D_T$. The Stokes-Einstein equation describes the translational diffusion coefficient of a spherical fluorophore in solution (3D) as a function of temperature (T), the Boltzmann constant (k_B), and the hydrodynamic radius (a) of the diffusing species such that $D_T = k_B T / 6\pi\eta a$ (20). The autocorrelation curves were analyzed using OriginPro 7 and the fit goodness was judged by both the residual (not shown) and χ^2 ($\leq$0.001). In the hydrodynamic model by Saffman and Delbrück (33), the translational diffusion coefficient of a transmembrane protein in a lipid bilayer depends on the viscosity (of both membrane, η_m, and surrounding solvent, η_w), membrane thickness (h), and protein radius (a) such that:

$$D_T = \frac{k_B T}{4\pi\eta_m h}[\ln(\eta_m h/\eta_w a) - 0.5772] \quad (9)$$

In addition, the model also provides a theoretical prediction for the translational/rotational diffusion coefficient ratio (D_T / D_R), which depends quadratically on the hydrodynamic radius of the diffusing protein in a lipid bilayer (33):

$$D_T/D_R = [\ln(\eta_m h/\eta_w a) - 0.5772]a^2 \quad (10)$$

In this hydrodynamic model, the membrane was treated as a Newtonian fluid layer (with a constant viscosity and perfectly flat surface over large distances) for a purely two-dimensional flow. Here, we use both Saffman-Delbrück (Eq. 10) and Stokes-Einstein (where, $D_T / D_R = 4a^2 / 3$) models to compare our experimental results on Bdp-Chol with the calculated translational/rotational diffusion coefficient ratio.

RESULTS AND DISCUSSION

Bdp-Chol partitions into liquid-ordered domains

To examine Bdp-Chol partitioning into various lipid phases, we first conducted confocal microscopy on GUVs comprised of various molar ratios of DOPC, SM, and cholesterol (Table 1 and Fig. 2). This ternary lipid mixture was chosen to mimic the outer leaflet of eukaryotic plasma membranes (34,35). The specific lipid compositions were determined from the published phase diagram for DOPC/SM/cholesterol in GUVs at 23°C (36). We first examined the Bdp-Chol partitioning in ternary GUVs with coexisting L_o and L_d phases. A previous report showed that partitioning of Bdp-Chol is sensitive to the N-acyl chain composition of SM (11). The egg SM used here contains a number of N-acyl chain lengths ranging from 16:0 to 24:0, but is predominantly (~84%) 16:0. The L_d domains in GUVs were labeled with DiI-C_{12} (34,37–39) in addition to Bdp-Chol. In contrast to the L_d domain specificity of DiI-C_{12}, Bdp-Chol partitions into both L_o and L_d domains, albeit with an approximately twofold enhancement in fluorescence intensity (i.e., concentration, not quantum yield, as shown below using fluorescence lifetime imaging) in the L_o phase. These findings differ slightly from a recent AFM-confocal study on supported lipid bilayers (11). In their study, Shaw et al. (11) used (in part) N-C18:0-SM, DOPC, and Bdp-Chol to form supported planar bilayers by in situ fusion onto a substrate. The use of different SMs and possible substrate effects may contribute to the differences in Bdp-Chol partitioning into L_o and L_d domains in our GUVs versus the supported bilayer studies (11). The miscibility behavior of lipids in supported bilayers may additionally contribute to the different partitioning of Bdp-Chol in GUVs (40).

We also examined the partitioning of Bdp-Chol (0.08 mol %) between the L_d and L_β phase. In binary GUVs comprised of a 1:1 mixture of DOPC and sphingomyelin (41), we observed negligible partitioning of Bdp-Chol into the L_β phase, which is consistent with previous calorimetric studies on liposomes (42). In their studies, Spink et al. found that cholesterol favors the L_β phase with $K_p = 3.3$ for DPPC. Cholesterol was insoluble in the gel phase, where it forms a separate phase or domain (43), which may be responsible for the small patches of fluorescence that we observed on our GUVs (Fig. 2 *C*). Confocal images of vesicles with various compositions, show that Bdp-Chol appears to partition in a fashion similar to that of unlabeled cholesterol.

Fluorescence lifetime-based FRET efficiency and phase-partitioning of Bdp-Chol

The spectral overlap (Fig. 1 *B*) between the emission of Bdp-Chol (donor) and the absorption of DiI-C_{12} (acceptor) suggests that these lipid analogs may form a FRET pair. Assuming randomly distributed dipoles (i.e., orientation parameter, $\kappa^2 = 2/3$), this spectral overlap yields an estimated Förster critical distance (R_0) of ~2.04 nm. We used time-resolved fluorescence measurements (2P FLIM and single-point modalities) to quantify the corresponding FRET efficiency (E) and intermolecular interactions between these lipid analogs (Fig. 3). Of particular interest is the use of lifetime-based FRET studies to probe lateral heterogeneity and partitioning of Bdp-Chol in ternary GUVs. The results also provide structural information on Bdp-Chol orientation in the lipid bilayer relative to DiI-C_{12} (5).

2P FLIM for FRET analysis

Previously, we have shown that the fluorescence lifetime of Bdp-PC (i.e., a tail-labeled lipid without cholesterol) is a sensitive probe of lipid order, particularly in the hydrophobic region of the bilayer, in single-phase DOPC (L_d) and DPPC (L_β) vesicles (5). 2P FLIM images of L_o-L_d coexisting domains in ternary GUVs labeled only with Bdp-Chol show slightly different lifetimes between the two lipid phases (Fig. S1 in Supporting Material). Using pixel-to-pixel lifetime analyses (Fig. S1 *C*), for example, the fluorescence lifetime of Bdp-Chol in the L_d domain is found to be shorter (4.5 $\pm$ 0.4 ns) than that in the L_o domain (5.5 $\pm$ 0.2 ns). In these FLIM analyses, the Bdp-Chol fluorescence/pixel (binning = 5) decays as a single exponential (considering the signal/noise ratio and temporal resolution), independent of the lipid phase.

In the presence of DiI-C_{12} in the L_d phase of ternary GUVs (Fig. 3 *A*), 2P FLIM images show a more distinct fluorescence

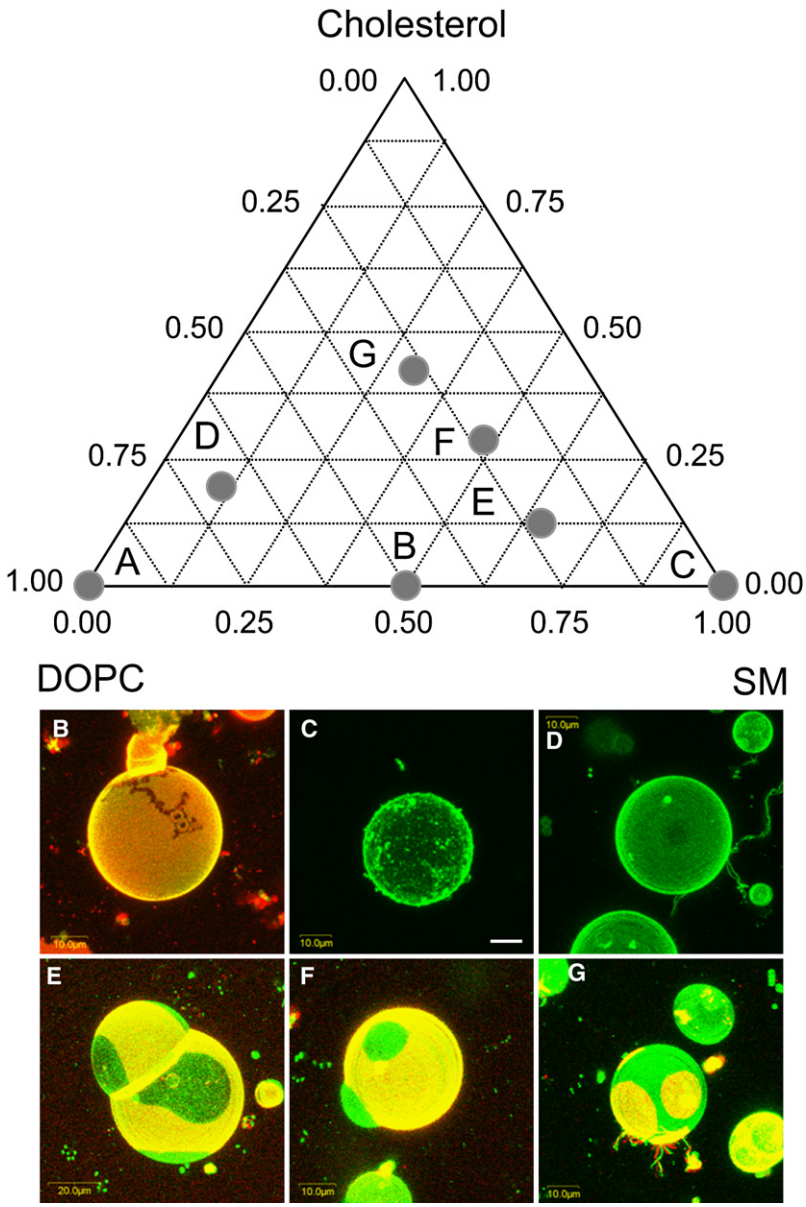

FIGURE 2 The formation and coexistence of lipid phase domains in GUVs are sensitive to lipid mixing. (*Top*) The phase diagram of DOPC/SM/Chol at 23°C (36) served as our guide for the lipid compositions (*D*, L_o phase; *E–G*, L_o-L_d coexistence; *B*, L_o-L_β coexistence; *C*, L_β phase). (*Bottom*) Confocal images of GUVs of varying lipid composition (*B–G*; see Table 2) labeled with Bdp-Chol and DiI-C_{12}. DiI-C_{12} is known to partition into the L_d phase (*red*), whereas Bdp-Chol partitions into both L_o and L_d phases (*green*). In the L_d phase, there is colocalization of DiI-C_{12} and Bdp-Chol (*yellow*). Bdp-Chol is excluded from the gel (L_β) phase. Scale bar, 10 μm.

lifetime of Bdp-Chol in the L_o–L_d coexisting domains (Fig. 3 *B*). The corresponding lifetime-pixel histogram (Fig. 3 *C*) can be described by a double Gaussian fit where each peak corresponds to the L_o ($\tau_1 = 5.40$ ns, width = 0.98 ns, amplitude = 1085, and area under band = 64%) and L_d ($\tau_2 = 3.96$ ns, width = 0.89 ns, amplitude 742, and area under band = 36%) phases, respectively, that coexist in this particular ternary GUV. Additional pixel-to-pixel lifetime analyses indicate that the fluorescence lifetime of Bdp-Chol in the L_o domain is 5.5 ± 0.4 ns, as compared with 3.8 ± 0.2 ns in the L_d domain in the presence of DiI-C_{12}. The 2P FLIM studies of Bdp-Chol, in the presence and absence of DiI-C_{12}, indicate energy transfer between this likely donor-acceptor pair (Fig. 3), which supports our predictions based on their spectral overlap (Fig. 1 *B*). Based on these FLIM measurements, the estimated FRET efficiency in L_d domains is 0.19 ± 0.07, with an average donor-acceptor distance (R) of 2.6 ± 0.2 nm (Fig. 3). To confirm these findings with high signal/noise ratio and enhanced temporal resolution, we also conducted 1P single-point time-resolved fluorescence measurements where the laser was strategically focused on a selected lipid domain.

1P single-point fluorescence lifetime measurements for FRET analysis

Single-point, 1P fluorescence of Bdp-Chol in DMSO decays as a single exponential fluorescence with a time constant of 4.62 ± 0.02 ns. In the sucrose buffer of GUVs, the Bdp-Chol fluorescence decays as a triexponential with an average lifetime of $\overline{\tau}_{fl} = 1.87 \pm 0.08$ ns, likely due to micelle formation, which enables us to rule out any significant contribution of the free analog. Complementary measurements of Bdp-Chol in

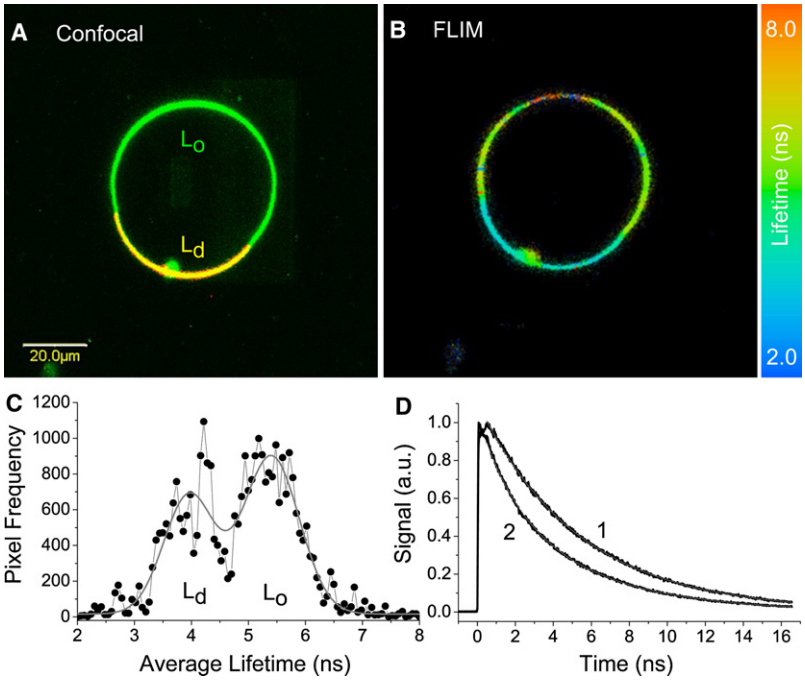

FIGURE 3 Fluorescence lifetime imaging of Bdp-Chol is sensitive to the lipid domains in liquid-liquid coexisting vesicles, especially in the presence of the L_d label DiI-C_{12}. (*A*) Complementary two-channel confocal imaging of DiI-C_{12} and Bdp-Chol enables us to identify the L_d and L_o phase domains, respectively, in ternary GUVs. (*B*) The corresponding 2P FLIM images of Bdp-Chol reveal a shorter lifetime in the L_d phase, especially in the presence of DiI-C_{12}, due to FRET. (*C*) A pixel-lifetime histogram of the FRET image shows a bimodal distribution, with each peak representative of each lipid phase domain. Using a double Gaussian fit (see text) of this histogram, the lifetime distribution peaks at ~4.2 ns and ~5.3 ns, which is consistent with the single-point lifetime measurements for the L_d and L_o phases, respectively. (*D*) Using single-point, 1P excitation (480 nm, 4.2 MHz), the Bdp-Chol fluorescence in L_o (*curve 1*) and L_d (*curve 2*, in the presence of DiI-C_{12}) phase domains decays as a biexponential with distinct average lifetime due to FRET (Table 2). During these single-point measurements, the laser was strategically focused on the domain of interest.

single-phase L_d GUVs show that fluorescence decays with an average lifetime ($\overline{\tau}_{fl} = 5.34 \pm 0.08$ ns) similar to that in the L_o phase (5.57 ± 0.07 ns). The Bdp-Chol fluorescence decays biexponentially in the L_β-phase GUVs with an average lifetime of 5.2 ± 0.1 ns and spatial heterogeneity that is likely due to lipid packing effects (43). These average lifetimes of Bdp-Chol are similar to literature values of Bdp-PC (without the cholesterol) in GUVs (15). In ternary vesicles with L_d-L_o phase coexistence, we also examined GUVs with "barbell" shapes where a slightly longer lifetime (5.53 ± 0.09 ns) was measured at one end of the barbell, compared with 5.38 ± 0.06 ns at the other end. Based on these fluorescence lifetime measurements on single- and ternary-phase GUVs, we conclude that the fluorescence lifetime of Bdp-Chol is slightly shorter in the L_d phase than in the L_o phase (see Table 2 for a summary).

TABLE 2 Fitting parameters for single-point fluorescence lifetime measurements on Bdp-Chol-labeled GUVs

Lipid composition*	τ_1 (ns)†	α_1	τ_2 (ns)	α_2	$\overline{\tau}$ (ns)
L_d (A), $n = 9$	5.0 (1)	0.81 (3)	7.9 (3)	0.19 (3)	5.50 (8)
L_d (B)‡, $n = 8$	1.8 (2)	0.28 (6)	5.4 (1)	0.72 (5)	4.5 (4)
L_β (C), $n = 5$	2.9 (2)	0.38 (5)	6.6 (2)	0.62 (5)	5.2 (1)
L_o (D), $n = 8$	—	—	5.5 (1)	1.00	5.5 (1)
L_o (E-G)§, $n = 10$	4.6 (2)	0.33 (2)	5.6 (4)	0.65 (4)	5.27 (8)
L_d (E-G)‡, $n = 12$	1.8 (3)	0.29 (3)	5.3 (1)	0.71 (3)	4.3 (1)

Numbers in parentheses represent the standard deviations of the last digit.
*See Table 1 for details of lipid compositions.
†The deconvoluted fluorescence decays, measured at magic-angle (54.7°) polarization, were fitted using a nonlinear least-squares fitting routine with reduced $\chi^2 = 1.0$–1.3.
‡A small fraction of DiI-C_{12} was present in the L_d-phase domain, but the fluorescence excitation and detection were optimized for Bdp-Chol.
§L_d and L_β phases coexist in samples E–G (see Table 1).

With only a slight difference in Bdp-Chol fluorescence lifetime in L_d and L_o domains, its general use as a viable contrasting agent in liquid-liquid domain coexistence studies may be hampered. Interestingly, however, this limitation was easily overcome using 1P fluorescence lifetime imaging of Bdp-Chol in ternary GUVs where the L_d domain is also labeled with DiI-C_{12} (Fig. 3 *D*). In coexisting liquid-liquid GUVs, the lifetime of Bdp-Chol in the L_o phase is 5.27 ± 0.08 ns in the absence of DiI-C_{12} (Fig. 3 *D*, *curve 1*) and is significantly reduced to 4.1 ± 0.4 ns in the presence of DiI-C12 (acceptor) (Fig. 3 *D*, *curve 2*), presumably due to FRET. Using these Bdp-Chol fluorescence lifetimes in the presence and absence of DiI-C_{12}, we estimate a FRET efficiency of 0.25 and a donor-acceptor distance of ~2.45 nm in the L_d phase.

The efficient FRET between Bdp-Chol (donor) and DiI-C_{12} (acceptor, L_d-specific label) allows us to calculate the Bdp-Chol partitioning between different lipid phases using fluorescence lifetime imaging. For example, single-point fluorescence decay parameters of Bdp-Chol, in the presence of DiI-C_{12} (Table 2), enabled us to calculate the partitioning of these lipid analogs into L_o and L_d phase domains. The estimated partitioning coefficient (K_p^a ~0.35) for DiI-C_{12} suggests a high affinity of this lipid analog for the disordered phase. The value calculated here is slightly higher than that reported previously ($K_p^a = 0.15 \pm 0.02$) (44), which may be attributed to the different lipids used in the two studies. In contrast, Bdp-Chol exhibits a high affinity for the L_o phase with K_p^d ~1.8, which is consistent with enhanced affinity for the ordered phase, as shown in the confocal images.

In addition to Bdp-Chol partitioning into lipid domains, the observed FRET with DiI-C_{12} provides insight into

donor-acceptor dipole configurations (i.e., intermolecular distance and dipolar orientation) in the lipid bilayer. We previously showed that the dipole of DiI-C_{12} is mostly aligned parallel to the polar headgroups of the phospholipids while sampling the immediate aqueous environment adjacent to the bilayer (5). The Bodipy dipole will be 2.6 ± 0.2 nm in the hydrophobic core of each leaflet while the hydroxyl group of cholesterol is in the phospholipid headgroup region (see below). It is important to note that the longer dipole of Bdp-Chol fluorophore is likely to be perpendicular to the acyl chains within the hydrophobic core of the bilayer, whereas the shorter dipole will be parallel to the acyl chains. Finally, these results highlight the potential of Bdp-Chol and DiI-C_{12} as a FRET pair for studying translational heterogeneity and cholesterol-rich, in vivo L_o domains below the diffraction limit.

Enhanced membrane fluidity and lipid order of liquid-ordered phase domains as probed using rotational diffusion of Bdp-Chol

To examine the lipid order and membrane fluidity of membrane domains, we carried out steady-state (Fig. 4) and time-resolved (Fig. 5) fluorescence anisotropy measurements on Bdp-Chol in phase-specific GUVs. These measurements also enabled us to examine the randomized dipole orientation assumption (i.e., $\kappa^2 = 2/3$) for the donor-acceptor pairs in our FRET analysis.

Steady-state anisotropy imaging

To assess the degree of order in lipid domains and the distribution of Bdp-Chol dipoles (with respect to the laser polarization), we used simultaneous parallel and perpendicular 2P fluorescence polarization imaging of Bdp-Chol in ternary GUVs to calculate the steady-state anisotropy per pixel. A typical 2P anisotropy image of Bdp-Chol in liquid-liquid domains is shown in Fig. 4 *B*. The corresponding confocal image of the same ternary GUV is also shown to help specifically identify the L_d (DiI-C_{12}) and L_o (Bdp-Chol) phase domains (Fig. 4 *A*). These results clearly indicate distinct environmental restrictions and higher order of Bdp-Chol in the L_o phase ($\langle r_0\ (x,\ y)\rangle = 0.4 \pm 0.1$) compared with the L_d phase ($\langle r_0\ (x,\ y)\rangle = 0.22 \pm 0.05$) (Fig. 4 *B*). The angular dependence of 2P anisotropy indicates photoselectivity of Bdp-Chol excitation and, therefore, a high degree of Bdp-Chol order in the lipid bilayer. Such an angular distribution of Bdp-Chol anisotropy contrasts with the homogenous anisotropy of Bdp-PC alone (i.e., without cholesterol) in L_d and L_β GUVs (5). In the presence of DiI-C_{12} in the L_d phase, the reduced initial anisotropy of Bdp-Chol can be attributed to either fast energy transfer (20) or domain-specific restriction on the tumbling motion of this analog in disordered lipid domains. However, similar trends are

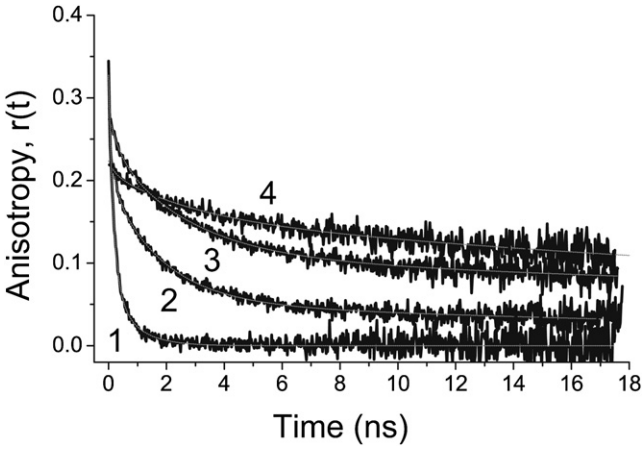

FIGURE 5 Rotational diffusion of Bdp-Chol directly reports on membrane fluidity of lipid domains in GUVs. Time-resolved fluorescence anisotropy of Bdp-Chol (in DMSO, 2 cP, 295 K) decays as a biexponential with $\varphi_1 = 0.18$ ns, $\beta_1 = 0.252$, $\varphi_2 = 0.8$ ns, and $\beta_2 = 0.077$ (*curve 1*). Time-resolved anisotropy of Bdp-Chol in single L_d phase GUVs decays as a triple exponential with $\varphi_1 = 0.15$ ns, $\beta_1 = 0.07$, $\varphi_2 = 1.8$ ns, $\beta_2 = 0.15$, $\varphi_3 = 38.6$ ns, and $\beta_3 = 0.05$ (*curve 2*). In L_o domains of ternary GUVs, the anisotropy of Bdp-Chol also decays as a triexponential with $\varphi_1 = 0.37$ ns, $\beta_1 = 0.05$, $\varphi_2 = 2.8$ ns, $\beta_2 = 0.15$, $\varphi_3 = 56.5$ ns, and $\beta_3 = 0.07$ (*curve 3*). The rotational diffusion of Bdp-Chol in the L_β phase decays as a biexponential with a significantly slow average rotational time (*curve 4*). The fitting parameters and statistics of Bdp-Chol rotational diffusion in GUVs are summarized in Table 3.

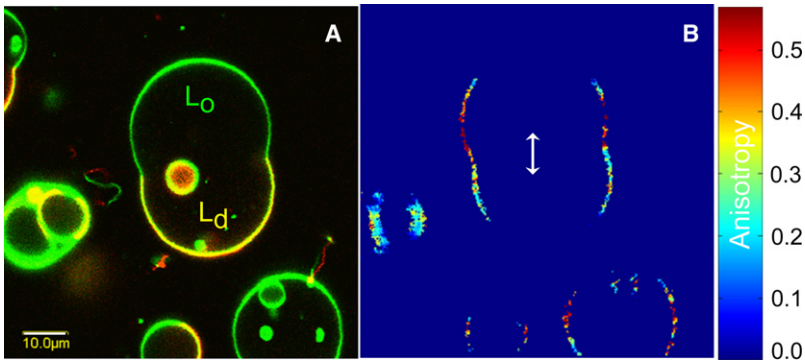

FIGURE 4 Coexisting liquid-liquid domains, labeled with Bdp-Chol, exhibit distinct steady- state 2P anisotropy imaging in ternary GUVs and in the presence of the L_d label, DiI-C_{12}. (*A*) Complementary two-channel confocal imaging of DiI-C_{12} and Bdp-Chol enables us to identify the coexisting L_d and L_o phase domains, respectively, in ternary GUVs. (*B*) The corresponding 2P fluorescence polarization images (both parallel and perpendicular) were recorded simultaneously, and the anisotropy image was calculated. The steady-state anisotropy/pixel, $r(x,y)$, of Bdp-Chol is lower in the L_d phase (0.22 ± 0.05) compared to the L_o phase (0.4 ± 0.1), which indicates a lower degree of lipid order. The reduction of $r(x,y)$ in the L_d phase domain seems independent of the DiI-C_{12} presence (Fig. S2). The arrow indicates the laser polarization. The color bar represents the steady-state 2P anisotropy.

also observed in vesicles that are only labeled with Bdp-Chol (Fig. S2), i.e., in the absence of DiI-C_{12} in the L_d domain. This observation suggests that L_d and L_o domains exhibit different lipid order and, therefore, different degrees of restriction on Bdp-Chol mobility. The corresponding angular difference between the absorbing and emitting dipoles (20) of Bdp-Chol is 41 ± 2° and 36 ± 4° in the L_d and L_o domains, respectively, showing greater conformational flexibility in Bdp-Chol in the L_d domain. As a result, fluorescence polarization imaging of Bdp-Chol can be used to contrast liquid-liquid domain coexistence.

The observed angular distribution of Bdp-Chol suggests a high degree of order in the lipid bilayer, where the Bdp dipole is oriented somewhat perpendicular to the phospholipid acyl chains. This Bdp orientation is consistent with the above mentioned FRET with DiI-C_{12}, as well as previous molecular dynamics simulations (45,46), NMR (47), and neutron diffraction studies (48,49), which have shown that the cholesterol hydroxyl group is energetically favored to be near the phospholipid polar headgroups (i.e., near the lipid-water interface). To assess the transbilayer distribution of Bdp-Chol in the GUV bilayer, we performed preliminary quenching experiments using trypan blue, which is impermeable to membranes (50). In the presence of 0.0075% (w/v) of trypan blue quencher, the Bdp-Chol cross-sectional fluorescence intensity per vesicle was reduced by ~40% (Fig. S3). These results suggest that only Bdp-Chol in the outer leaflet of the GUVs bilayer is accessible to the trypan blue quenching, whereas the remaining ~60% of this cholesterol analog is within the inner leaflet of GUVs and thus remains unquenched.

Time-resolved fluorescence anisotropy

We used single-point time-resolved anisotropy measurements to quantify the rotational diffusion of Bdp-Chol in lipid domains and the corresponding membrane fluidity ($1/\eta$, where η is the microviscosity at a given temperature T in Kelvin) (51–53). In addition, the amplitude of the anisotropy decay components is used to calculate the orientation parameter ($S = \sqrt{r_\infty / r_0}$, or $S = \sqrt{\beta_{slow}/r_0}$) (20), which reflects the bilayer constraint on the rotational motion of lipid analogs (54–56). As a control, the anisotropy of Bdp-Chol in DMSO (η = 2 cP, 295 K) decays as a biexponential (φ_1 = 0.18 ns, β_1 = 0.252, φ_2 = 0.8 ns, and β_2 = 0.077) with an average rotational time ($\overline{\varphi}$) of 0.32 ns and initial anisotropy (r_0) of 0.329 (Fig. 5, *curve 1*). Using the Stokes-Einstein model for a spherical fluorophore and the measured average rotational time, the estimated hydrodynamic radius of Bd-Chol is 0.54 nm, which is consistent with theoretical calculations (0.55 nm) based on the molecular weight (20) of Bdp-Chol (576.41). The rotational diffusion coefficient ($D_R = 1/6\overline{\varphi}$) of Bdp-Chol is $5.2 \times 10^8\ s^{-1}$ and $2.1 \times 10^8\ s^{-1}$ in DMSO using the average and slow (φ_2) rotational time constants, respectively. In the GUV buffer (sucrose), however, the anisotropy of Bdp-Chol decays as a biexponential (φ_1 = 1.8 ns, β_1 = 0.025, φ_2 = 19.0 ns, and β_2 = 0.025) with an average rotational time of 0.52 ns and much reduced initial anisotropy (r_0 = 0.05). Taking into consideration the overall rotational time constant, we estimate a likely micelle radius of 2.5 ± 0.3 nm in sucrose. In addition, the distinct anisotropy decay enables us to rule out a significant contribution of a free Bdp-Chol in the GUV buffer.

Time-resolved anisotropy of Bdp-Chol in single-L_d-phase GUVs decays as a triple exponential with φ_1 = 0.15 ns, β_1 = 0.07, φ_2 = 1.8 ns, β_2 = 0.15, φ_3 = 38.6 ns, and β_3 = 0.05 (Fig. 5, *curve 2*). The average rotational time of 8.2 ± 0.3 ns yields a rotational diffusion coefficient of $(2.0 \pm 0.1) \times 10^7\ s^{-1}$, compared with $(4.9 \pm 0.7) \times 10^6\ s^{-1}$ for the slow rotational component. The observed fast tumbling motion of Bdp-Chol validates our random dipole orientation assumption ($\kappa^2 = 2/3$) in FRET analysis. This temporal randomization of Bdp-Chol, as well as of DiI-C_{12} (5), facilitates Förster resonance energy transfer between this donor-acceptor pair, even in a highly organized structure such as a lipid bilayer. Further calculations of the order parameter show that Bdp-Chol dipoles are ordered ($S = 0.45 \pm 0.04$) in single-phase L_d GUVs (Table 3). This order parameter compares well with electron spin resonance experiments, which report ''averaged'' order parameters (unlike nuclear magnetic resonance) (57) in DOPC bilayers (58,59). Time-resolved fluorescence anisotropy measurements are sensitive to fast segmental mobility (e.g., the tumbling motion of Bdp), as

TABLE 3 Time-resolved fluorescence anisotropy decays of Bdp-Chol in GUVs of varying composition

Environment*	φ_1 (ns)	β_1	φ_2 (ns)	β_2	φ_3 (ns)	β_3	r_0	$\overline{\varphi}$ (ns)	S
DMSO; $n = 4$	0.18 (2)*	0.25 (1)	0.8 (1)	0.08 (1)	—	—	0.33 (1)	0.33 (3)	—
L_d (A); $n = 12$	0.15 (2)*	0.07 (2)	2.5 (6)	0.14 (1)	35 (5)	0.05 (1)	0.25 (3)	8.2 (3)	0.45 (4)†
L_β (C); $n = 3$	—	—	3.2 (3)	0.19 (2)	52 (3)	0.18 (2)	0.37	26 (3)	0.7 (2)
L_o (D); $n = 4$	0.37 (9)	0.05 (1)	2.8 (7)	0.15 (1)	56 (2)	0.07 (2)	0.27 (1)	16.3 (4)	0.52 (5)
L_o (E–G)‡; $n = 8$	0.3 (1)	0.05 (1)	2.9 (9)	0.11 (2)	48 (3)	0.11 (5)	0.27 (5)	20.8 (7)	0.63 (9)
L_d (E–G); $n = 8$	0.4 (1)	0.04 (1)	2.7 (3)	0.11 (2)	44 (2)	0.10 (5)	0.25 (4)	18.9 (3)	0.53 (9)

Numbers in parentheses represent the standard deviations of the last digit.

*For details of GUV composition, see Table 2.

†The sum of preexponential factors (i.e., r_0) and the slow-component amplitude (β_3) of the anisotropy decay were used to calculate the order parameters (S). The time-resolved anisotropy decays were fitted using a nonlinear least-squares fitting routine (OriginPro7) with $\chi^2 \leq 0.005$.

‡L_d and L_β phases coexist in samples E–G (see Table 1).

well as overall rotational diffusion of Bdp-Chol. As a result, use of the average rotational time may underestimate lipid bilayer microviscosity. Accordingly, we used both the average and slow rotational time constants to calculate the corresponding rotational diffusion coefficient and membrane microviscosity. Assuming that Bdp-Chol is a sphere with a radius of 0.54 nm, the apparent microviscosity of the DOPC fluid domain is 49 ± 1 cP (i.e., fluidity of ~2.1 P^{-1} at room temperature) based on the average rotational time, which agrees with values in other studies (60–63) in which different lipid types and fluorescent analogs were used. However, in using the average rotational time, the fast rotational components may be too fast to sample Bdp-Chol friction with other lipid molecules in the bilayer, thus underestimating the microviscosity. In contrast, the slow rotational time component of Bdp-Chol in the DOPC bilayer yields an estimated microviscosity of 232 ± 7 cP (i.e., fluidity of ~0.43 P^{-1}), which agrees with other literature values (64,65). This wide range of microviscosity values of bilayers can be attributed to the variation of lipid types and experimental techniques employed in previous studies.

In L_o domains of ternary GUVs, the Bdp-Chol anisotropy (Fig. 5, *curve 3*) also decays as a triexponential (φ_1 = 0.37 ns, β_1= 0.05, φ_2 = 2.8 ns, β_2= 0.15, φ_3 = 56.5 ns, and β_3= 0.07) with an estimated average rotational time, $\overline{\varphi}$ = 16.3 ± 0.4 ns, that is significantly ($p < 0.05$) different from that in the L_d phase ($\overline{\varphi}$ ~ 8.2 ns). The average rotational time yields a rotational diffusion coefficient of (1.0 ± 0.4) × 10^7 s^{-1}, compared with (2.9 ± 0.2) × 10^6 s^{-1}, which corresponds to the slow rotational component. These results suggest a hindered Bdp-Chol rotational motion in the presence of more highly ordered saturated acyl chains in L_o domains. For a spherical Bdp-Chol with a radius of 0.54 nm, the apparent microviscosity of the L_o domain is 98 ± 0.2 cP (i.e., fluidity of ~1.1 P^{-1} at room temperature) based on the average rotational time, as compared with 339 ± 9 cP (i.e., fluidity of 0.3 P^{-1}) using the slow rotational component. The estimated order parameter in L_o domains (S = 0.52 ± 0.05) is significantly larger than in the L_d domain (0.43 ± 0.03), which agrees with previous reports (66,67). The L_β phase in single-phase GUVs ($S = 0.7 \pm 0.2$) exhibits a slow average rotational time (26 ± 3 ns) with a rate of (6.4 ± 0.5) × 10^6 s^{-1}, compared with (3.2 ± 0.2) × 10^6 s^{-1} for the slow component (Fig. 5, *curve 4*). Systematic investigation of rotational diffusion as a function of the experimental geometry will facilitate assignment of the observed rotational time constants to presumably out-of-plane and in-plane motions of Bdp-Chol within the bilayer and is an objective of current studies. Under the experimental geometry used in these studies, however, the observed three-exponential anisotropy decays and order parameters ($S < 1.0$) indicate a mixture of in-plane and out-of-plane rotational modes (20) of Bdp-Chol dipole (16) with respect to the lipid bilayer. The fitting parameters of Bdp-Chol rotational diffusion in GUV lipid domains are summarized in Table 3.

Translational diffusion of Bdp-Chol reveals lipid phase sensitivity: comparison with fast rotational diffusion

To test the hypothesis of cholesterol-lipid complex formation (4) and the validity of the Saffman-Delbrück model (33) for describing the diffusion of a cholesterol derivative in a lipid bilayer, we carried out complementary translational diffusion measurements of Bdp-Chol in lipid domains using FCS. Together with our rotational diffusion analysis described above (Table 3), the experimental D_T / D_R value of Bdp-Chol will be compared with the theoretical predictions using both the hydrodynamic (Eq. 10) and Stokes-Einstein models. For a spherical fluorophore diffusing in solution (i.e., Stokes-Einstein model for 3D), the translational-to-rotational diffusion coefficient ratio depends quadratically on its hydrodynamic radius ($D_T / D_R = 4a^2 / 3$) but is independent of the surrounding viscosity as described in the seminal article by Saffman and Delbrück (33). However, time-resolved fluorescence anisotropy measurements, unlike those made with FCS, are sensitive to fast segmental mobility as well as overall rotational diffusion. As a result, we use both the average and the slow rotational time constants of Bdp-Chol to calculate its rotational diffusion coefficient in lipid domains. Using these multiscale diffusion measurements and the corresponding temporal-to-spatial scaling (hence short- and long-range diffusion), one would expect that the rotational diffusion of a molecule spans shorter (or microscopic) distances when compared with long-range (or macroscopic) translational diffusion (17). This spatiotemporal scaling may also be important in differentiating between Brownian and non-Brownian (or anomalous) diffusion in biological membranes due to molecular crowding, transmembrane proteins, and cytoskeletal confinement.

As a control, the fluorescence fluctuation autocorrelation of Bdp-Chol was measured in DMSO ($\eta = 2$ cP at 295 K, $\tau_D = 0.43 \pm 0.07$ ms (Fig. 6, *curve 2*)) with an estimated translational diffusion coefficient of (5.4 ± 0.2) × 10^{-7} cm^2/s, using RhG (phosphate-buffered saline (PBS), $\eta = 0.89$ cP, $\tau_D = 0.08 \pm 0.01$ ms, $D_T = 2.8 \times 10^{-6}$ cm^2/s) as a reference (Fig. 6, *curve 1*). Using both translational and slow rotational diffusion coefficients, the experimental D_T/D_R value for Bdp-Chol (in DMSO) is 0.26 ± 0.03 nm^2, which yields a hydrodynamic radius of 0.51 ± 0.06 nm (Table 4). Based on the molecular weight of Bdp-Chol (576.41), we calculated a hydrodynamic radius of 0.55 nm assuming a spherical shape (20), which agrees well with our experimental estimate of 0.54 nm.

In the L_d domain in DOPC vesicles, a typical fluorescence fluctuation autocorrelation of Bdp-Chol is shown in Fig. 6 (*curve 3*) and can be described using a 2D autocorrelation function (Eq. 8). The measured translational diffusion time (τ_D) of Bdp-Chol in the L_d phase is 3.1 ± 0.7 ms with an estimated D_T = (7.4 ± 0.3) × 10^{-8} cm^2/s (n = 12). As mentioned above, the rotational diffusion coefficient of

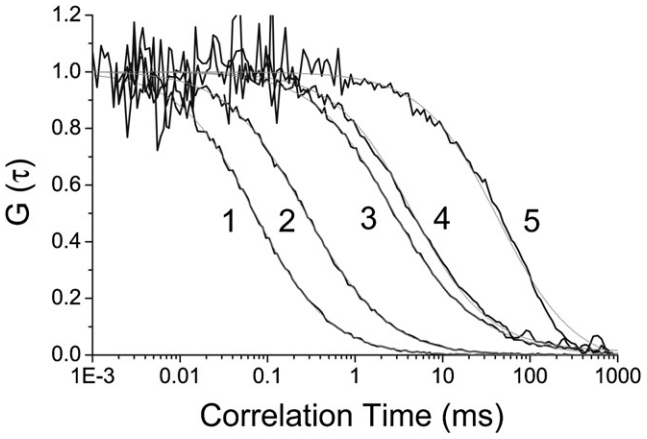

FIGURE 6 Translational diffusion of Bdp-Chol in GUVs is lipid-domain-sensitive as measured using fluorescence correlation spectroscopy. The autocorrelation function of RhG (in PBS, pH 7.4, 0.89 cP, 295 K; *curve 1*) and Bdp-Chol (in DMSO, 2 cP, 295 K; *curve 2*) are described well using diffusion alone (Eq. 7), with diffusion times of 0.08 ± 0.01 ms and 0.43 ± 0.07 ms, respectively. A typical autocorrelation curve of Bdp-Chol in the L_d domain is also shown, using single-phase L_d GUVs (*curve 3*), as compared with the L_o (*curve 4*) and L_β (*curve 5*) phase domains (see Table 4 and text). These autocorrelation curves are normalized for visual comparison of the phase dependence of Bdp-Chol translational diffusion time and diffusion coefficient in lipid bilayers. The dotted lines (*gray*) are the fit curves (Eq. 7: RhG in PBS and Bdp-Chol in DMSO; Eq. 8: Bdp-Chol in lipid phase domains) that yielded the best χ^2 (<0.0005) and residual (not shown).

Bdp-Chol in DOPC (L_d phase) GUVs is $(2.0-0.4) \times 10^7\ s^{-1}$. Accordingly, the experimental translational/rotational coefficient ratio, D_T/D_R, for Bdp-Chol is $0.24 \pm 0.09\ nm^2$ in the L_d phase. The corresponding autocorrelation curves of Bdp-Chol in L_o (composition D: DOPC/SM/Chol = 70:10:20; τ_D = 4.5 ± 0.8 ms (Fig. 6, *curve 4*)) and L_β (composition C: DOPC/SM/Chol = 0:100:0; τ_D = 64 ± 17 ms (Fig. 6, *curve 5*)) domains indicate slow translational diffusion coefficients of $(5.0 \pm 0.2) \times 10^{-8}\ cm^2/s$ and $(3.5 \pm 0.1) \times 10^{-9}\ cm^2/s$, respectively. Based on the average ($1.0 \times 10^7\ s^{-1}$) and slow ($2.9 \times 10^6\ s^{-1}$) rotational coefficients of Bdp-Chol in L_o domains, the experimental D_T/D_R ratio is $0.77 \pm 0.05\ nm^2$. Using fluorescence fluctuation autocorrelation, the translational diffusion time (τ_D = 11 ± 2 ms) and diffusion coefficient ($1.9 \pm 0.1 \times 10^{-8}\ cm^2/s$) of Bdp-Chol in liquid-liquid coexisting domains (G: DOPC/SM/Chol = 25:40:35) were also measured (see Table 4).

As mentioned above, based on theoretical calculations, the estimated hydrodynamic radius of a spherical Bdp-Chol (576.41 Da) is 0.55 nm. In addition, the viscosity of the lipid bilayer (thickness, $h \sim 3.5$ nm) and the surrounding buffer is $\eta_m = 47 - 225$ cP (for the L_d domain; see above) and η_w = 0.89 cP, respectively (Table 4). Using Eq. 10 with the above parameters, we predict that $D_T/D_R = 1.9 \pm 0.3\ nm^2$ for Bdp-Chol in L_d domains. This ratio is larger than the experimental value of $0.24 \pm 0.09\ nm^2$ for the same L_d phase. Such a discrepancy between theoretical expectations from the Saffman-Delbrück model and the experimental results could be attributed to measured translational (macroscopic) diffusion (and therefore D_T/D_R) of Bdp-Chol being slower than predicted because the analog forms a complex with phospholipids. However, the size of such phospholipid/cholesterol complexes is likely to be small (2.7 ± 0.5 nm, i.e., Bdp-Chol complex with a few phospholipids), in agreement with a thermodynamic model of condensed complexes by Anderson and McConnell (13). Care must be taken, however, since the hydrodynamic model for transmembrane proteins such as rhodopsin in the Saffman and Delbrück report (33) may not be applicable to a small lipid analog

TABLE 4 Experimental and calculated values of the translational-to-rotational diffusion coefficient ratio (D_L / D_R) of Bdp-Chol in different environments (at 295 K)

				$D_T/D_R(nm^2)$		
				Experimental	Theoretical‡	
Fluorophore	Environment	$D_R(s^{-1})$*	$D_T(cm^2/s)$†		SD (2D)	SE (3D)
RhG	PBS (0.89 cP)	1.3×10^9	2.8×10^{-6}	0.22 ± 0.02	—	0.346
Bdp-Chol	DMSO (2 cP)	5.2×10^8	5.41×10^{-7}	0.11 ± 0.02	—	0.403§
		2.1×10^8	—	0.26 ± 0.04	—	0.403
	L_d phase	2.0×10^7	7.23×10^{-8}	0.36 ± 0.02	1.61	0.403
		4.9×10^6	—	1.48 ± 0.02	2.08	0.403
	L_β phase	6.4×10^6	3.5×10^{-9}	0.06 ± 0.01	2.15	0.403
		3.2×10^6	—	0.11 ± 0.03	2.16	0.403
	L_o phase	1.0×10^7	4.98×10^{-8}	0.46 ± 0.06	1.81	0.403
		2.9×10^6	—	1.1 ± 0.6	2.19	0.403

*The rotational diffusion coefficient was calculated using the average ($\overline{\varphi}$, top number) and slow (φ_3, bottom number) rotational times of Bdp-Chol in the lipid bilayer measured by time-resolved anisotropy.

†The translational diffusion coefficient was calculated using the diffusion times of Bdp-Chol in lipid bilayer measured by FCS.

‡The theoretical D_T/D_R ratio was calculated using the Saffman and Delbrück (*SD*) (Eq. 10) and Stokes-Einstein (*SE*) models for 2D and 3D diffusion, respectively. In these calculations, we used membrane microviscosity (η_m) as estimated by time-resolved anisotropy, buffer viscosity η_w = 0.89 cP, and membrane thickness h = 3.5 nm.

§The hydrodynamic radius of Bdp-Chol used in these calculations was calculated using its rotational time constant (Stokes-Einstein model in DMSO) and molecular weight.

such as Bdp-Chol and its occupancy in a single leaflet of the lipid bilayer. It is of interest, and provides support for this argument, that the predicted D_T / D_R ratio (0.4 nm^2) for Bdp-Chol in the L_d phase, using the Stokes-Einstein model, is relatively closer to the experimental value (Table 4). Recent experimental studies on various peptides and transmembrane proteins in 1-stearoyl-2-oleoyl-*sn*-glycero-3-phosphocholine GUVs have suggested that the measured translational diffusion coefficient disagree with the predicted values using the Saffman-Delbrück model (64). The authors also indicate that their experimental results agree with a heuristic Stokes-Einstein-like expression that is weighted by a characteristic length for dimensional reasons. Mesoscopic simulation studies have also been reported to quantify the size-dependent diffusion properties of membrane inclusions (65). These simulations suggest that the Saffman-Delbrück model (Eq. 9) describes well the translational diffusion of molecules with a smaller radius than the critical value of $h\eta_m / 2\eta_w \approx 7.4$ nm. However, the authors reported significant deviations from the hydrodynamic model for molecules with a radius larger than the critical value (65). In contrast to the lateral diffusion, the authors also reported that the size dependence of the rotational diffusion coefficient (D_R) follows the predicted hydrodynamic scaling over the entire size range studied.

CONCLUSIONS

Using an integrated fluorescence-dynamics assay and ternary GUVs, we have shown that Bdp-Chol is a useful analog for a wide range of studies on membrane domains. Supported by our experimental data, this cholesterol analog adopts the same conformation as the parent cholesterol molecule itself, thereby partitioning into lipid phases in the same manner (i.e., with the Bdp moiety in the hydrophobic core and the hydroxyl group of cholesterol aligned close to the polar headgroups of phospholipids). Our results show that Bdp-Chol partitions preferentially into the L_o phase, as compared with the L_d and L_β domains. Fluorescence lifetime imaging of Bdp-Chol is sensitive to lipid domains. It is important to note that the observed lifetime-based FRET efficiency between Bdp-Chol and DiI-C_{12} indicates a potential of this new cholesterol analog for studying membrane heterogeneity beyond the diffraction limit of optical microscopy. The rotational diffusion analyses of this new analog also indicate a highly ordered phase with distinct membrane fluidity in the L_o domains. Comparative FCS studies of Bdp-Chol translational diffusion in bilayers indicate a single-diffusing species with a diffusion coefficient that is sensitive to the lipid phase. This contrasts with the rotational diffusion studies that suggest Bdp-Chol experiences a heterogeneous conformation and microenvironment on the ps–ns timescale. The measured and calculated ratio of translational and rotational diffusion coefficients of Bdp-Chol also indicates a likely formation of cholesterol-lipid complexes during its macroscopic (translational) diffusion. Our findings open the door for the use of this fluorescent cholesterol analog in studying many aspects of membranes under controlled changes in thermodynamic parameters.

SUPPORTING MATERIAL

Three figures are available at http://www.biophysj.org/biophysj/supplemental/S0006-3495(09)00390-7.

We are grateful to Dr. Michael Edidin (Department of Biology, Johns Hopkins University, Baltimore, MD) for a thoughtful discussion. We thank Angel Davey (Chemistry, Penn State University, University Park, PA) and Qianru Yu (Bioengineering, Penn State University, University Park, PA) for their careful reading and editing of this manuscript.

This work was supported by National Science Foundation grant MCB0718741 (A.A.H.) and National Institutes of Health grant AG030949 (A.A.H.). Additional support was provided by National Institutes of Health grant HL-083187 (to R.B.), the Penn State Materials Research Institute, and the Penn State Materials Research Science and Engineering Center (supported by National Science Foundation grant DMR-0213623), and the Lehigh-Penn State Center for Optical Technologies (supported by the Commonwealth of Pennsylvania).

REFERENCES

1. Bagatolli, L. A., and E. Gratton. 2000. Two photon fluorescence microscopy of coexisting lipid domains in giant unilamellar vesicles of binary phospholipid mixtures. *Biophys. J.* 78:290–305.
2. Leidy, C., W. F. Wolkers, K. Jorgensen, O. G. Mouritsen, and J. H. Crowe. 2001. Lateral organization and domain formation in a two-component lipid membrane system. *Biophys. J.* 80:1819–1828.
3. Wang, T.-Y., R. Leventis, and J. R. Silvius. 2000. Fluorescence-based evaluation of the partitioning of lipids and lipidated peptides into liquid-ordered lipid microdomains: a model for molecular partitioning into "lipid rafts". *Biophys. J.* 79:919–933.
4. Feigenson, G. W. 2007. Phase boundaries and biological membranes. *Annu. Rev. Biophys. Biomol. Struct.* 36:63–77.
5. Ariola, F. S., D. J. Mudaliar, R. P. Walvick, and A. A. Heikal. 2006. Dynamics imaging of lipid phases and lipid-marker interactions in model biomembranes. *Phys. Chem. Chem. Phys.* 39:4517–4529.
6. Davey, A. M., R. P. Walvick, Y. Liu, A. A. Heikal, and E. D. Sheets. 2007. Membrane order and molecular dynamics associated with IgE receptor cross-linking in mast cells. *Biophys. J.* 92:343–355.
7. Gidwani, A., D. Holowka, and B. Baird. 2001. Fluorescence anisotropy measurements of lipid order in plasma membranes and lipid rafts from RBL-2H3 mast cells. *Biochemistry.* 40:12422–12429.
8. Hess, S. T., E. D. Sheets, A. Wagenknecht-Wiesner, and A. A. Heikal. 2003. Quantitative analysis of the fluorescence properties of intrinsically fluorescent proteins in living cells. *Biophys. J.* 85:2566–2580.
9. Sinha, M., S. Mishra, and P. G. Joshi. 2003. Liquid-ordered microdomains in lipid rafts and plasma membrane of U-87 MG cells: a time-resolved fluorescence study. *Eur. Biophys. J.* 32:381–391.
10. Haluska, C. K., A. P. Schroder, P. Didier, D. Heissler, G. Duportail, et al. 2008. Combining fluorescence lifetime and polarization microscopy to discriminate phase separated domains in giant unilamellar vesicles. *Biophys. J.* 95:5737–5747.
11. Shaw, J. E., R. F. Epand, R. M. Epand, Z. Li, R. Bittman, et al. 2006. Correlated fluorescence-atomic force microscopy of membrane domains: structure of fluorescence probes determines lipid localization. *Biophys. J.* 90:2170–2178.
12. Anderson, T. G., and H. M. McConnell. 2001. Condensed complexes and the calorimetry of cholesterol-phospholipid bilayers. *Biophys. J.* 81:2774–2785.

13. Anderson, T. G., and H. M. McConnell. 2002. A thermodynamic model for extended complexes of cholesterol and phospholipid. *Biophys. J.* 83:2039–2052.

14. Li, Z., E. Mintzer, and R. Bittman. 2006. First synthesis of free cholesterol-BODIPY conjugates. *J. Org. Chem.* 71:1718–1721.

15. Karolin, J., L. B.-A. Johansson, L. Strandberg, and T. Ny. 1994. Fluorescence and absorption spectroscopic properties of dypyrrommetheneboron difluoride (BODIPY) derivatives in liquids, lipid membranes, and proteins. *J. Am. Chem. Soc.* 116:7801–7806.

16. Bergstrom, F., I. Mikhalyov, P. Hagglof, R. Wortmann, T. Ny, et al. 2002. Dimers of dipyrrometheneboron difluoride (BODIPY) with light spectroscopic applications in chemistry and biology. *J. Am. Chem. Soc.* 142:196–204.

17. Saxton, M. J., and K. Jacobson. 1997. Single-particle tracking: applications to membrane dynamics. *Annu. Rev. Biophys. Biomol. Struct.* 26:373–399.

18. Yu, Q., M. Proia, and A. A. Heikal. 2008. Integrated biophotonics approach for non-invasive, multiscale studies of biomolecular and cellular biophysics. *J. Biomed. Opt.* 13:1–14, 041315.

19. O'Connor, D. V., and D. Phillips. 1984. Time-Correlated Single Photon Counting. Academic Press, London.

20. Lakowicz, J. 2006. Principles of Fluorescence Spectroscopy. Springer, Singapore.

21. Volkmer, A., V. Subramaniam, D. J. S. Birch, and T. M. Jovin. 2000. One- and two-photon excited fluorescence lifetimes and anisotropy decays of green fluorescent proteins. *Biophys. J.* 78:1589–1598.

22. Axelrod, D. 1979. Carbocyanine dye orientation in red-cell membrane studied by microscopic fluorescence polarization. *Biophys. J.* 26:557–573.

23. Axelrod, D. 1989. Fluorescence polarization microscopy. *Methods Cell Biol.* 30:333–352.

24. Loura, L. M. S., A. Fedorov, and M. Prieto. 2001. Fluid-fluid membrane microheterogeneity: a fluorescence resonance energy transfer study. *Biophys. J.* 80:776–788.

25. Santos, N. C., M. Prieto, and M. A. R. B. Castanho. 2003. Quantifying molecular partition into model systems of biomembranes: an emphasis on optical spectroscopic methods. *Biochim. Biophys. Acta.* 1612:123–135.

26. Marsh, D. 1990. Handbook of Lipid Bilayers. CRC Press, Boca Raton, FL.

27. Hess, S. T., S. Huang, A. A. Heikal, and W. W. Webb. 2002. Biological and chemical applications of fluorescence correlation spectroscopy: a review. *Biochemistry.* 41:697–705.

28. Heikal, A. A., S. T. Hess, G. S. Baird, R. Y. Tsien, and W. W. Webb. 2000. Molecular spectroscopy and dynamics of intrinsically fluorescent proteins: coral red (dsRed) and yellow (Citrine). *Proc. Natl. Acad. Sci. USA.* 97:11996–12001.

29. Visser, N. V., M. A. Hink, A. v. Hoek, and A. J. W. G. Visser. 1999. Comparison between fluorescence correlation spectroscopy and time-resolved fluorescence anisotropy as illustrated with a fluorescent dextran conjugate. *J. Fluoresc.* 9:251–255.

30. Haupts, U., S. Maiti, P. Schwille, and W. W. Webb. 1998. Dynamics of fluorescence fluctuations in green fluorescent protein observed by fluorescence correlation spectroscopy. *Proc. Natl. Acad. Sci. USA.* 95:13573–13578.

31. Ries, J., and P. Schwille. 2008. New concepts for fluorescence correlation spectroscopy on membranes. *Phys. Chem. Chem. Phys.* 10:3487–3497.

32. Sengupta, P., J. Balaji, and S. Maiti. 2002. Measuring diffusion in cell membranes by fluorescence correlation spectroscopy. *Methods.* 27:374–387.

33. Saffman, P. G., and M. Delbruck. 1975. Brownian motion in biological membranes. *Proc. Natl. Acad. Sci. USA.* 72:3111–3113.

34. Hammond, A. T., F. A. Heberle, T. Baumgart, D. Holowka, B. Baird, et al. 2005. Crosslinking a lipid raft component triggers liquid ordered-liquid disordered phase separation in model plasma membranes. *Proc. Natl. Acad. Sci. USA.* 102:6320–6325.

35. Silvius, J. R. 2003. Fluorescence energy transfer reveals microdomain formation at physiological temperatures in lipid mixtures modeling the outer leaflet of the plasma membrane. *Biophys. J.* 85:1034–1045.

36. Veatch, S. L., and S. L. Keller. 2002. Organization in lipid membranes containing cholesterol. *Phys. Rev. Lett.* 89:268101–268105.

37. Baumgart, T., G. Hunt, E. R. Farkas, W. W. Webb, and G. W. Feigenson. 2007. Fluorescence probe partitioning between L_o/L_d phases in lipid membranes. *Biochim. Biophys. Acta.* 1768:2182–2194.

38. Spink, C. H., M. D. Yeager, and G. W. Feigenson. 1990. Partitioning behavior of indocarbocyanine probes between coexisting gel and fluid phases in model membranes. *Biochim. Biophys. Acta.* 1023:25–33.

39. Wustner, D. 2007. Plasma membrane sterol distribution resembles the surface topography of living cells. *Mol. Biol. Cell.* 18:211–228.

40. Stottrup, B. L., S. L. Veatch, and S. L. Keller. 2004. Nonequilibrium behavior in supported lipid membranes containing cholesterol. *Biophys. J.* 86:2942–2950.

41. Wang, T. -Y., and J. R. Silvius. 2003. Sphingolipid partitioning into ordered domains in cholesterol-free and cholesterol-containing lipid bilayers. *Biophys. J.* 84:367–378.

42. Spink, C. H., S. Manley, and M. Breed. 1996. Thermodynamics of transfer of cholesterol from gel to fluid phases of phospholipid bilayers. *Biochim. Biophys. Acta.* 1279:190–196.

43. Harris, J. S., D. E. Epps, S. R. Davio, and F. J. Kezdy. 1995. Evidence for transbilayer, tail-to-tail cholesterol dimers in dipalmitoylglycerophosphocholine liposomes. *Biochemistry.* 34:3851–3857.

44. Vaz, W. L. C., and E. Melo. 2001. Fluorescence spectroscopic studies on phase heterogeneity in lipid bilayer membranes. *J. Fluoresc.* 11:255–271.

45. Kessel, A., N. Ben-Tal, and S. May. 2001. Interactions of cholesterol with lipid bilayers: the preferred configuration and fluctuations. *Biophys. J.* 81:643–658.

46. Robinson, A. J., W. G. Richards, P. J. Thomas, and M. M. Hann. 1995. Behavior of cholesterol and its effect on head group and chain conformations in lipid bilayers: a molecular dynamics study. *Biophys. J.* 68:164–170.

47. Daragan, V. A., A. M. Voloshin, S. V. Chochina, T. N. Khazanovich, W. G. Wood, et al. 2000. Specific binding of ethanol to cholesterol in organic solvents. *Biophys. J.* 79:406–415.

48. Worcester, D. L., and N. P. Franks. 1976. Structural analysis of hydrated egg lecithin and cholesterol bilayers. II. Neutron diffraction. *J. Mol. Biol.* 100:359–378.

49. Endress, E., H. Heller, H. Casalta, M. F. Brown, and T. M. Bayerl. 2002. Anisotropic motion and molecular dynamics of cholesterol, lanosterol, and ergosterol in lecithin bilayers studied by quasi-elastic neutron scattering. *Biochemistry.* 41:13078–13086.

50. Papadopoulos, A., S. Vehring, I. Lopez-Montero, L. Kutschenko, M. Stockl, et al. 2007. Flippase activity detected with unlabeled lipids by shape changes of giant unilamellar vesicles. *J. Biol. Chem.* 282: 15559–15568.

51. Mejía, R., M. C. Gómez-Eichelmann, and M. S. Fernández. 1995. Membrane fluidity of *Escherichia coli* during heat-shock. *Biochim. Biophys. Acta.* 1239:195–200.

52. Ohmori, T., Y. Kimura, N. Hirota, and M. Terazima. 2003. Diffusion of transient radicals in alcohols and cyclohexane from ambient to supercritical conditions studied by the transient grating method. *J. Phys. Chem. B.* 107:5958–5966.

53. Swallen, S. F., P. A. Bonvallet, R. J. McMahon, and M. D. Ediger. 2003. Self-diffusion of tris-Naphthylbenzene near the glass transition temperature. *Phys. Rev. Lett.* 90, 015901/1–4.

54. Kinosita, K., A. Ikegami, and S. Kawato. 1982. On the wobbling-in-cone analysis of fluorescence anisotropy decay. *Biophys. J.* 37: 461–464.

55. Krishna, M. M. G., A. Srivastava, and N. Periasamy. 2001. Rotational dynamics of surface probes in lipid vesicles. *Biophys. Chem.* 90: 123–133.

56. Lipari, G., and A. Szabo. 1980. Effect of librational motion on fluorescence depolarization and nuclear magnetic resonance relaxation in macromolecules and membranes. *Biophys. J.* 30:489–506.

57. Engel, L. W., and F. G. Prendergast. 1981. Values for and significance of order parameters and ''cone angles'' of fluorophore rotation in lipid bilayers. *Biochemistry.* 20:7338–7345.

58. East, J. M., O. T. Jones, A. C. Simmonds, and A. G. Lee. 1984. Membrane fluidity is not an important physiological regulator of the (Ca^{2+}-Mg^{2+})-dependent ATPase of sarcoplasmic reticulum. *J. Biol. Chem.* 259:8070–8071.

59. Bonosi, F., G. Gabrielli, E. Margheri, and G. Martini. 1990. Effect of the addition of ceramide to dioleoylphosphatidylcholine vesicles: an ESR and SEM study. *Langmuir.* 6:1769–1773.

60. Wagner, R., E. Apley, A. Gross, and U. I. Flugge. 1989. The rotational diffusion of chloroplast phosphate translocator and of lipid molecules in bilayer membranes. *Eur. J. Biochem.* 182:165–173.

61. Koan, M. M., and G. J. Blanchard. 2006. Gauging the effect of impurities on lipid bilayer phase transition temperature. *J. Phys. Chem. B.* 110:16584–16590.

62. Shafirovich, V. Y., E. E. Batova, and P. P. Levin. 1995. Monitoring of molecular dynamics in liquid bilayers of small unilamellar vesicles by magnetic-field-sensitive probes. *J. Am. Chem. Soc.* 117:6093–6100.

63. Yun, I., S. K. Han, S. W. Baik, N. H. Kim, J. S. Kang, et al. 1988. Effects of local anesthetics on the fluidity of synaptosomal plasma membrane vesicles isolated from bovine brain. *Korean J. Pharmacol.* 24:43–52.

64. Gambin, Y., R. Lopez-Esparza, M. Reffay, E. Sierecki, N. S. Gov, et al. 2006. Lateral mobility of proteins in liquid membranes revisited. *Proc. Natl. Acad. Sci. USA.* 103:2098–2102.

65. Guigas, G., and M. Weiss. 2006. Size-dependent diffusion of membrane inclusions. *Biophys. J.* 91:2393–2398.

66. Hao, Y. H., and J. W. Chen. 2001. Influence of cholesterol on the biophysical properties of the sphingomyelin/DOPC binary system. *J. Membr. Biol.* 183:85–92.

67. Rog, T., and M. Pasenkiewicz-Gierula. 2006. Cholesterol-sphingomyelin interactions: a molecular dynamics simulation study. *Biophys. J.* 91:3756–3767.